Wall charge effects on structural properties of a coarse-grained FENE polyelectrolyte confined in slit nanochannels by Brownian dynamics simulation

Jonggu Jeon and Myung-Suk Chun*

Complex Fluids Research Lab., Korea Institute of Science and Technology (KIST), 39-1 Hawolgok-dong, Seongbuk-gu, Seoul 136-791, Korea

Abstract

A polyelectrolyte chain confined in a slit nanochannel exhibits a structural transition from the one in free space. In this paper, the effect of the long-range electrostatic interactions between the xanthan polyelectrolyte and the slit wall on the confined xanthan conformation is investigated via the Brownian dynamics simulation. A neutral and two negatively charged surfaces of polydimethylsiloxane (PDMS) and glass are combined to make four kinds of slit channels with different charge characteristics: i) neutral-neutral, ii) glass-glass, iii) neutral-PDMS and iv) neutral-glass walls. Their walls are characterized by uniform surface charge densities determined from experimental data of zeta potential. Both the nonmonotonic chain size variation and the loss of long-range bond vector correlation, previously observed under confinement in the PDMS-PDMS slit, are also found in the neutral slit, demonstrating the nonelectrostatic origin of such crossover behaviors. As expected, the effect of wall charges is negligible at sufficiently high medium ionic strength of 100 mM but it becomes significant in the opposite limit of 0.01 mM. In the latter case, the high charge density of glass walls strengthens the effective confinement of a negatively charged polyelectrolyte and produces a xanthan structure comparable to that confined in a much narrower neutral slit. The obtained structural data suggest the possibility of controlling the structure of confined polyelectrolytes by the modification of surface charge characteristics of micro/nanofluidic devices in combination with the adjustment of the medium ionic strength.

Keywords : polyelectrolyte structure, slit nanochannel, finitely extendable nonlinear elastic (FENE), coarse-graining, Brownian dynamics simulation

1. Introduction

Polyelectrolytes confined in a micro/nanochannel environment exhibit altered structure and dynamics compared to their behavior in the bulk solution due to their interaction with the bounding surfaces. This confinement effect has practical relevance to the development of high-throughput micro total analysis system (μTAS) such as electrophoresis, micro-biochip, cell counting and single molecule detection (Chen *et al.*, 2004; Jo *et al.*, 2007).

The effect of one-dimensional confinement by two parallel walls on the structural and rheological properties of neutral and flexible polymer chains have previously been analyzed with theoretical and computational means. In particular, the theory of Daoud and de Gennes (1977) presents a scaling behavior of a confined polymer qualitatively different from Flory's celebrated bulk scaling law. Later, a more refined theory of Cordeiro *et al.* (1997) and lattice

Monte Carlo simulations (van Vliet and ten Brinke, 1990; Wang and Teraoka, 2000) have established that the crossover from unbounded to confined structure exhibits a nonmonotonic size variation with a minimum where the slit size is comparable to the chain end-to-end distance in bulk. In contrast, the structure of confined polyelectrolytes taking a finite rigidity due to intrachain electrostatic repulsion has been analyzed under two-dimensional confinement in a pore (Odijk, 1983; Brochard-Wyart *et al.*, 2005).

Brownian dynamics (BD) simulations of coarse-grained models have played important roles in understanding structural and rheological properties of polymers both in bulk solution (Allison, 1986; Öttinger, 1996; Jian *et al.*, 1997; Hur *et al.*, 2000) and under confinement (Jendrejack *et al.*, 2004; Hernandez-Ortiz *et al.*, 2007), providing information on, e.g., chain size, internal structure, translational and rotational dynamics, and chain stretch and migration in channels under flow.

Very recently, the authors have studied the structural transition of a polyelectrolyte chain from unbounded to confined states using the BD simulation with emphasis on

*Corresponding author: mschun@kist.re.kr

the influences of chain intrinsic rigidity and the ionic strength of the surrounding medium (Jeon and Chun, 2007). The confinement was influenced by the slit channel formed by two parallel plates with surface charge density similar to a level of polydimethylsiloxane (PDMS). This study found that the aforementioned nonmonotonic size variation is present in the confined polyelectrolytes with finite rigidity as well as in neutral and flexible chains and, moreover, the reduction in chain size at intermediate confinement is accompanied by severe loss of long-range bond vector correlation measured by the persistence length at long length scale. It also revealed that the effect of electrostatic interactions on the structural transition can reasonably be captured by the variable persistence length within the framework of wormlike chain theory.

In this paper, the structure of single polyelectrolyte chain confined in slit channels is investigated with channel walls of different surface charge densities. Three types of walls, representing neutral, PDMS, and glass surfaces, are considered and four different silt channels formed by them are used to assess their effects on the polyelectrolyte structure. By following our previous study, the electrostatic potential is described at the level of Debye-Hückel (DH) approximation. This will provide insights into i) how much of the confinement effect comes from the electrostatic repulsion between the polyelectrolyte and the wall as opposed to the steric repulsion between them and ii) the possibility of nano/microchannel design according to optimized wall charge characteristics with proper materials or coating.

2. Computational methodology

The computational methods similar to our previous study (Jeon and Chun, 2007) are employed except for the description of the asymmetric wall charge density for the neutral-PDMS and neutral-glass slits. Here, a brief review of the polyelectrolyte model and the BD simulation method is provided together with the DH description of the bead-wall electrostatic interaction in the asymmetrically charged slit.

2.1. Coarse-grained modeling of polyelectrolyte

We first develop a coarse-grained model of polyelectrolytes with polysaccharide xanthan as the model system. Xanthan is generally accepted as a semiflexible polymer at room temperature due to the double stranded structure with intrinsic persistence length of at least 100 nm (Paradossi and Brant, 1982; Sato et al., 1984; Sho et al., 1986; Chun and Park, 1994). It has up to two ionizable carboxyl groups per repeat unit.

The polyelectrolyte is modeled as a bead-spring chain with additional electrostatic, hydrodynamic and Lennard-Jones (LJ) interactions between beads. For the spring, the finitely extendable nonlinear elastic (FENE) potential of

Warner (1972) is employed as follows

$$E_{i,i+1}^{FENE} = -\left(\frac{k_S\, l_{max}^2}{2}\right)\ln\left[1-\left(\frac{r_{i,i+1}-l_0}{l_{max}}\right)^2\right] \qquad (1)$$

where $r_{i,i+1}$ is the distance between beads i and $i+1$, l_0 is the equilibrium bond length, and l_{max} is the maximum bond length allowed. In the limit of large l_{max}, E^{FENE} is reduced to a harmonic potential with force constant k_S (Tran-Canh and Tran-Cong, 2004). The dispersion-repulsion interaction between beads are taken into account by the standard LJ potential with parameters ε_{LJ} and σ_{LJ} set equal to the Boltzmann thermal energy $k_B T$ and l_0, respectively

$$E_{ij}^{LJ} = 4\varepsilon_{LJ}\left[\left(\frac{\sigma_{LJ}}{r_{ij}}\right)^{12}-\left(\frac{\sigma_{LJ}}{r_{ij}}\right)^6\right]. \qquad (2)$$

The electrostatic interaction between beads are described by the DH potential

$$E_{ij}^{ES} = \frac{q_b^2}{4\pi\varepsilon}\frac{e^{-\kappa r_{ij}}}{r_{ij}} = k_B T\, z_b^2 \frac{l_B}{r_{ij}}e^{-\kappa r_{ij}}. \qquad (3)$$

Here, q_b is the bead charge, $\varepsilon = \varepsilon_r\varepsilon_0$ is the electric permittivity of the medium defined in terms of dielectric constant ε_r and vacuum permittivity ε_0, $\kappa = (8\pi l_B N_A I)^{1/2}$ is the inverse Debye screening length defined in terms of Avogadro's number N_A and medium ionic strength I, $l_B = e^2/(4\pi\varepsilon k_B T)$ is the Bjerrum length (cf. $l_B = 0.71$ nm for water at room temperature, see Manning, 1969), and $z_b = q_b/e$ is the bead charge in units of positive elementary charge e (i.e., 1.6×10^{-19} C). The finite rigidity of the chain is modeled by the following harmonic bending potential

$$E_{i,i+1}^{Bend} = \frac{1}{2}k_A\theta_{i,i+1}^2; \quad \theta_{i,i+1} = \cos^{-1}(\hat{b}_i\cdot\hat{b}_{i+1}) \qquad (4)$$

where k_A is the bending force constant and $\hat{b}_i = (\mathbf{r}_{i+1}-\mathbf{r}_i)/|\mathbf{r}_{i+1}-\mathbf{r}_i|$ is the i-th bond vector of unit size.

A xanthan chain with molecular weight of 1.13×10^6 g/mol (~1220 monomers) has $l_P \cong 120$ nm and the contour length $R_C \cong 580$ nm at ionic strength $I = 100$ mM (Chun and Park, 1994). With the ratio $R_C/l_P \approx 5$, this chain can be regarded as a continuous wormlike chain. This is modeled as a discrete wormlike chain (Allison, 1986) with 25 beads ($N_b = 25$), with about 10 beads representing a Kuhn segment of length $2l_P$. This choice ensures a smooth persistence length variation with changing environmental conditions. The bead hydrodynamic radius a is chosen as 5 nm. The spring and charge parameters k_S, l_0, l_{max}, k_A and z_b are optimized with short BD simulations so that the chain in bulk solution reproduces experimental values of $R_C = 580$ and 880 nm and $l_P = 120$ and 200 nm at ionic strengths $I = 100$ and 0.2 mM, respectively. The optimized model parameters are summarized in Table 1.

2.2. Bead-wall interactions

As depicted in Fig. 1, the simulation of a confined chain

Table 1. Parameters of the model polyelectrolyte of xanthan chain and other simulation parameters

Number of beads, N_b (dimensionless)	25
Bead hydrodynamic radius, a (nm)	5.0
Bond bending force constant, k_A (k_BT)	4.0
Bond stretch force constant, k_S (k_BT/l_0^2)	2.5
Equilibrium bond length, l_0 (nm)	10.0
Maximum bond length, l_{max} (nm)	150.0
Bead charge, q_b (e)	−35.0
Lennard-Jones energy parameter, ε_{LJ} (k_BT)	1.0
Lennard-Jones size parameter, σ_{LJ} (l_0)	1.0
Surface charge density of wall, σ_W (C/m²)	0 (Neutral)
	−5.15×10⁻⁴ (PDMS)
	−1.03×10⁻³ (Glass)
Bead-wall steric force constant, k_W ($l_0^2 k_B T$)	2.5
Dielectric constant of aqueous medium, ε_r (dimensionless)	78.4
Viscosity of fluid, η (mPa·s)	0.89
Temperature, T (K)	298.15
Step size of simulation time, Δt (ns)	2.0
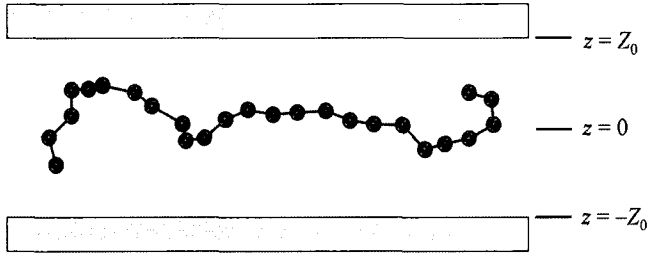
Fig. 1. A polyelectrolyte chain confined in the slit channel. The employed coordinate system is also shown.

requires the specification of the bead-wall interactions. For the bead-wall steric repulsion, the following empirical potential (Fernandes et al., 2000) is used for all three types of surfaces (i.e., neutral, PDMS and glass)

$$E_i^{WR} = \frac{k_W}{\left(|z_i| - Z_0\right)^2} \qquad (5)$$

with $k_W = 2.5 l_0^2 k_B T$ and Z_0 as the half-width of the slit. For the electrostatic potential, we employ the DH interaction of a point charge with two infinite charged plates. For a slit formed by two walls with surface charge density σ_1 (at $z = Z_0$) and σ_2 (at $z = -Z_0$), the electrostatic energy E_i^{WES} of bead i due to the walls is

$$E_i^{WES} = \frac{q_b}{\varepsilon \kappa \sinh(2\kappa Z_0)} \{\sigma_1 \cosh[\kappa(z_i + Z_0)] + \sigma_2 \cosh[\kappa(z_i - Z_0)]\} \qquad (6)$$

where z_i is the z coordinate of bead i with the z axis perpendicular to the walls and the origin at the center of the slit (see Fig. 1). This expression was obtained by solving the linearized Poisson-Boltzmann equation with the con-

stant charge condition at the walls. When the two walls have identical surface charge density σ_W, Eq. (6) is reduced to the expression used in our previous study. The surface charge density σ_W is set to −5.15×10⁻⁴ and −1.03×10⁻³ C/m² for the PDMS and glass walls, respectively. These values are very close to those determined from zeta potential ζ (cf. −18 and −36 mV for PDMS and glass, respectively) at solution pH 7.0, with the relationship $\sigma_W = \varepsilon \kappa \zeta$ (Russel, Saville and Schowalter, 1989; Chun and Lee, 2005). For simplicity, the ionic strength dependence of the wall charge density is not considered in the present study.

2.3. Brownian dynamics simulation

The generalized Langevin equation provides the reference for the generation of molecular trajectories. The dynamics of the polyelectrolyte chain is described by the following BD equation of motion that also accounts for the bead-bead hydrodynamic interaction (Ermak and McCammon, 1978)

$$\mathbf{r}_i^{n+1} = \mathbf{r}_i^n + \Delta t \sum_j \frac{\mathbf{D}_{ij}^n \cdot \mathbf{F}_j^n}{k_B T} + \Delta t \sum_j \nabla_j \cdot \mathbf{D}_{ij}^n + \mathbf{R}_i^n \qquad (7)$$

where $\mathbf{F}_j^n = -\nabla E^{Total}(t_n)$ is the force on bead i at time step n, $\mathbf{R}_i^n$ is the random displacement due to the solvent and Δt is the time step size. The Rotne-Prager diffusion tensor $\mathbf{D}_{ij}^n$ describes the hydrodynamic interaction between beads (Rotne and Prager, 1969). The distribution of $\mathbf{R}_i^n$ is Gaussian with zero mean and covariance, expressed as

$$\langle \mathbf{R}_i^n \mathbf{R}_j^n \rangle = 2\mathbf{D}_{ij}^n \Delta t \qquad (8)$$

where integration time step Δt is chosen as 2.0 ns. This satisfies the condition $m_0/(6\pi\eta a) \ll \Delta t \ll 6\pi\eta a^3/k_B T$, where η is the fluid viscosity and m_0 is the bead mass (Ermak and McCammon, 1978). In this study, the hydrodynamic interaction between the wall and the beads is not taken into account, but this does not alter structural properties in the absence of fluid flow.

For a given condition, 20 independent BD trajectories each of more than 10 ms in length are analyzed for properties. Structural properties such as the chain radius of gyration R_G, root-mean-square end-to-end distance R_E, contour length R_C and persistence length l_P, are determined with the following formulae (Doi and Edwards, 1986)

$$R_G^2 = \frac{1}{N_b} \sum_{n=1}^{N_b} \langle |\mathbf{r}_n - \mathbf{r}_{CM}|^2 \rangle; \quad \mathbf{r}_{CM} = \frac{1}{N_b} \sum_{n=1}^{N_b} \mathbf{r}_n, \qquad (9)$$

$$R_E = \langle \mathbf{R}_E^2 \rangle^{1/2}; \quad \mathbf{R}_E = \mathbf{r}_{N_b} - \mathbf{r}_1 = \sum_{n=1}^{N_b} \mathbf{r}_n, \qquad (10)$$

$$R_C = (N_b - 1)b = \sum_{n=1}^{N_b-1} b_n = \sum_{n=1}^{N_b-1} |\mathbf{r}_{n+1} - \mathbf{r}_n|, \qquad (11)$$

$$\frac{1}{N_b - n - 2} \left\langle \sum_{i=1}^{N_b-n-2} \hat{b}_i \cdot \hat{b}_{i+n} \right\rangle = \exp(-s_n/l_P^n), \qquad (12a)$$

$$s_n = \frac{1}{N_b - n} \left\langle \sum_{i=1}^{N_b-n} \sum_{m=1}^{n} |\mathbf{r}_{i+m} - \mathbf{r}_{i+m-1}| \right\rangle. \qquad (12b)$$

In Eqs. (9)-(12), the position of the center of mass $\mathbf{r}_{CM}$, the average bond length b, the length of n-th bond b_n, and the average contour distance between beads separated by n bonds s_n are also introduced. I_P^n becomes independent of n only when the bond vector correlation decays exponentially on the entire length scale. As written above, I_P^n provides a useful measure of the relative strength of the short- and long-range bond vector correlations. The translational self diffusion coefficient is calculated from the Einstein relation

$$D_T^\alpha = \lim_{t \to \infty} \frac{1}{2t} \left\langle [r_{CM}^\alpha(t+t_0) - r_{CM}^\alpha(t_0)]^2 \right\rangle \qquad (\alpha = x, y, z). \qquad (13)$$

To better reveal the effect of confinement on diffusivity, we consider only the two dimensional diffusion coefficient $D_T^{2D} = (D_T^x + D_T^y)/2$ both in bulk and under confinement. In practice, the limit $t \to \infty$ on the right-hand side of Eq. (13) is replaced by $t = 0.2$ ms. The estimated error from this choice is less than 2% in bulk solution and less than 5% under confinement.

The simulation system is infinite in the x and y directions and the size in the z direction is determined by the slit half-width Z_0, as depicted in Fig. 1. The system is not periodic because only a single chain is placed in the channel. The system is equilibrated for 2 ms (1×10^6 time steps) and the averages are taken for the next 14 ms (7×10^6 time steps).

3. Results and discussion

In this study, the medium ionic strength I and the channel half-width Z_0 are varied for each of the four slit nanochannels formed by the neutral-neutral (NN), neutral-PDMS (NP), neutral-glass (NG), glass-glass (GG) walls. Combined with our previous results on the PDMS-PDMS (PP) channel, the structure and the distribution of a confined polyelectrolyte chain in five different nanochannels are analyzed.

3.1. Effect of wall charges on the polyelectrolyte chain conformation

Figs. 2 and 3 display the chain size variation with the slit half-width Z_0 at three different I. The sigmoidal transitions of R_G and $(R_E/R_G)^2$ with Z_0 at $I = 0.01$ mM (Figs. 2a and 3a) and the nonmonotonic variation of the same quantities at higher I (Figs. 2b and 2c and Figs. 3b and 3c) are qualitatively the same as in Jeon and Chun (2007). This behavior arises because the model chain is rigid at the lowest I of 0.01 mM due to the intrachain electrostatic repulsion and this suppresses the nonmonotonic size variation of neutral flexible chain. On the other hand, semiflexible
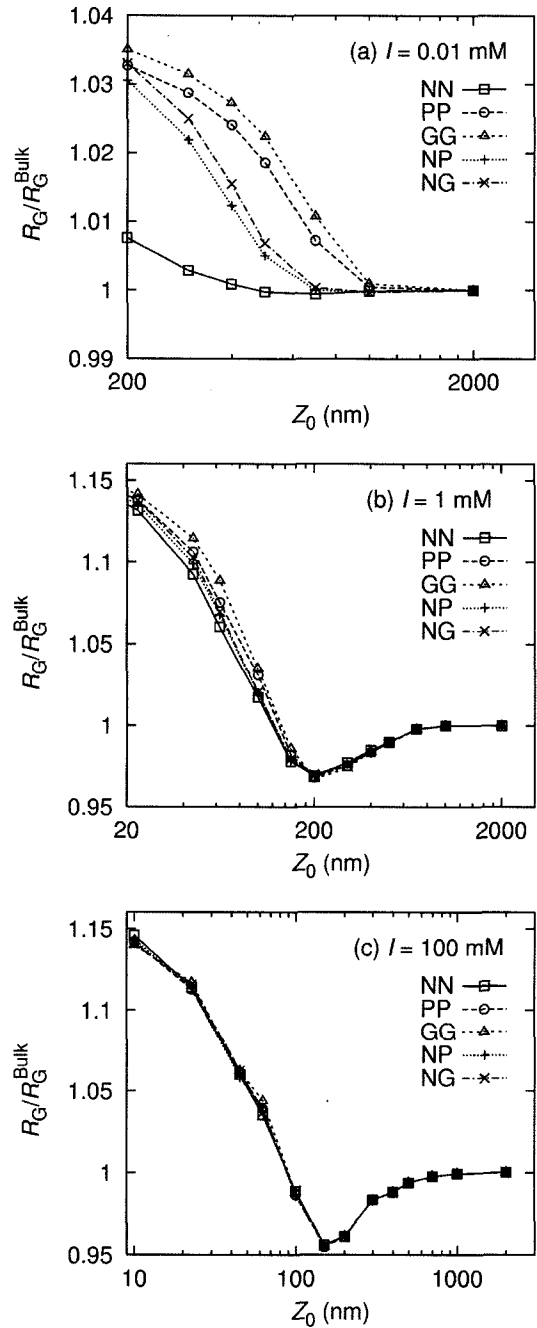

Fig. 2. The variation of the chain's radius of gyration R_G with slit half-width Z_0. The results from slits with different wall charges are shown for ionic strength (a) $I = 0.01$ mM, (b) $I = 1$ mM, and (c) $I = 100$ mM.

chains at intermediate and high I still possess a flexible nature and the nonmonotonic size variation is preserved.

The effect of the wall charges is most pronounced at $I = 0.01$ mM (Figs. 2a and 3a), where the structural transition takes place at a larger Z_0 as we go from the neutral NN channel to the highest charged GG channel. As expected from the strength of the bead-wall electrostatic repulsion, the degree of confinement is in the order NN, NP, NG, PP,
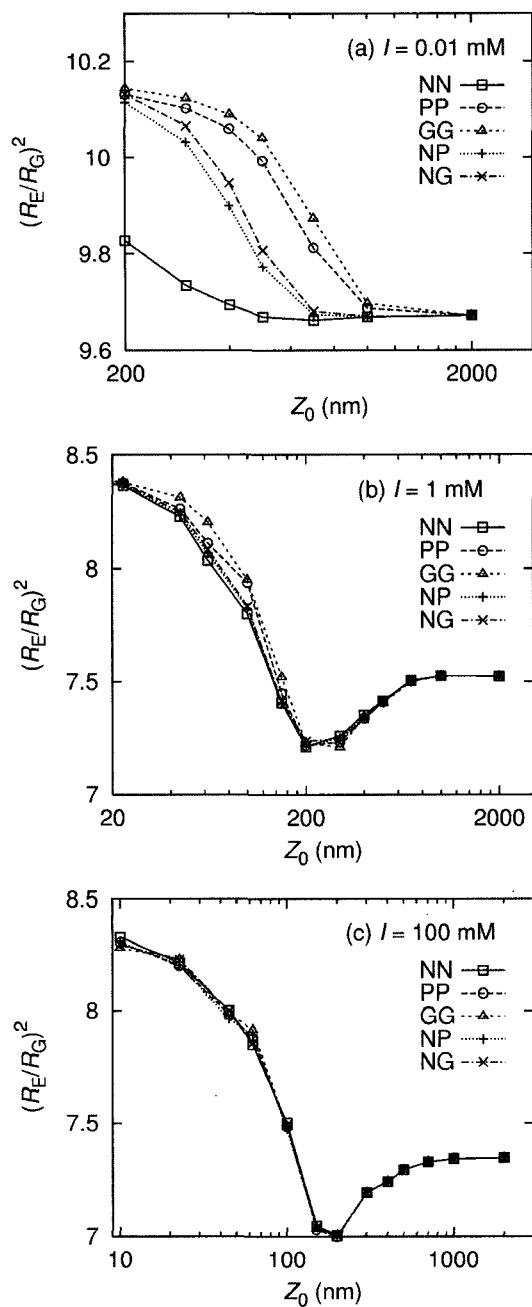
Fig. 3. The variation of the squared ratio of the end-to-end distance R_E to R_G with slit half-width Z_0. The results from slits with different wall charges are shown for ionic strength (a) $I = 0.01$ mM, (b) $I = 1$ mM, and (c) $I = 100$ mM.

Fig. 4. Dependence of the chain persistence length l_P^1 measured between neighboring beads on the slit half-width Z_0. Results at ionic strength (a) 0.01 mM and (b) 1 mM are provided.

and GG from the smallest to the largest. The differences in the effective confinement are very large. For example, the chain size in the GG channel with $Z_0 = 625$ nm is already larger than that in the NN channel with $Z_0 = 200$ nm. This suggests that a high degree of confinement of polyelectrolyte chains could suitably be achieved by the surface charge modification without relying on sophisticated fabrication processes. This effect is, however, significant only
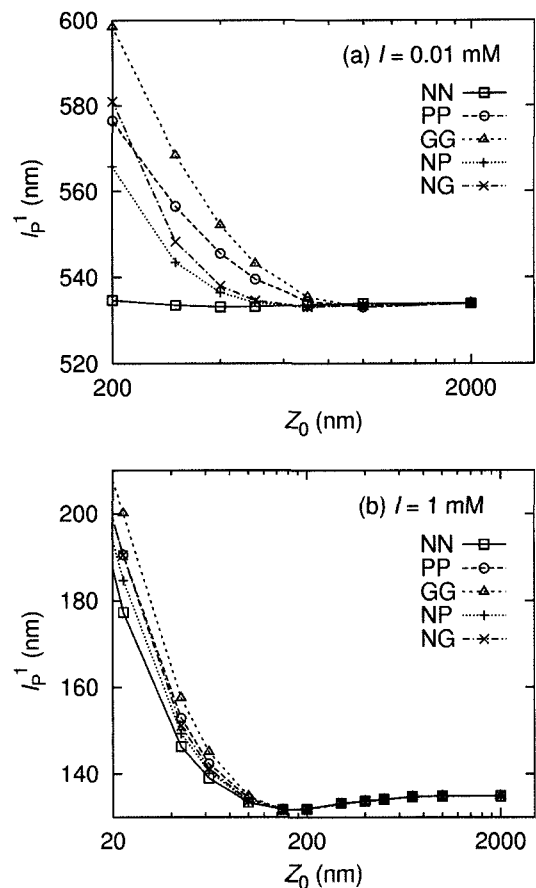
at low ionic strengths $I = 1$ mM, the effect of wall charges is quite small and is almost negligible at 100 mM (Figs. 2b and 2c and Figs. 3b and 3c). In these cases, the Debye screening length (κ^{-1} = 9.6 and 0.96 nm at $I = 1$ and 100 mM, respectively) is smaller than the average bead-wall distance (see Section 3.2) and the chain feels little effect of the wall charge.

Figs. 4 and 5 show the chain persistence length l_P^n at short ($n = 1$) and long ($n = 15$) length scales with different slit channels at $I = 0.01$ and 1 mM. As in the Figs. 2 and 3, the qualitative behavior of l_P^n is similar in all channels but the chain stretch (increase in l_P^n) is initiated at larger Z_0 as the wall charge increases. We note that the sudden decrease of l_P^{15} near $Z_0 = 200$-400 nm (Fig. 5b) represents the loss of long-range bond vector correlation at intermediate confinement. Remarkably, the magnitude of l_P^{15} in this region is in the order NN, NP, NG, PP, and GG from the largest to smallest, meaning that stronger electrostatic repulsion results in a smaller persistence length. This is contrary to the expectation based on the chain stretching effect of the bead-wall electrostatic repulsion, which would
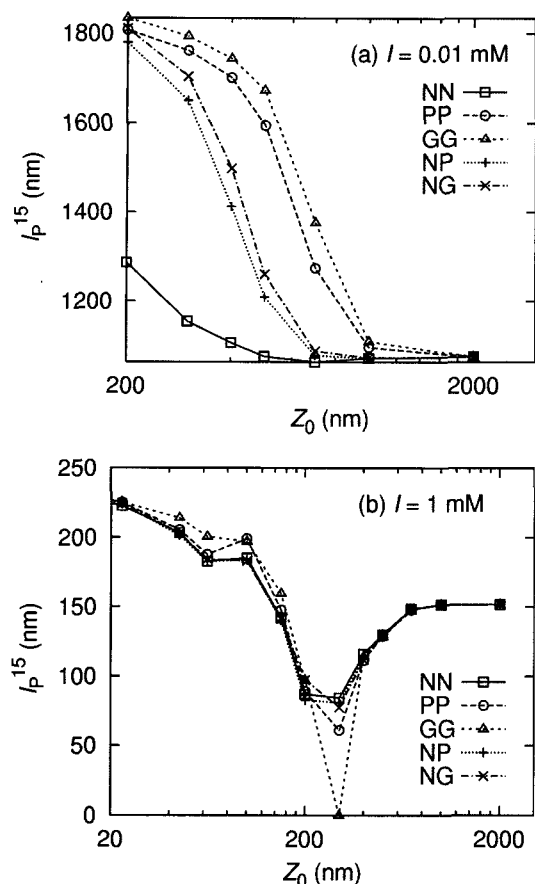
Fig. 5. Dependence of the chain persistence length l_P^{15} measured between beads separated by 15 bonds on the slit half-width Z_0. Results at ionic strength (a) 0.01 mM and (b) 1 mM are provided.
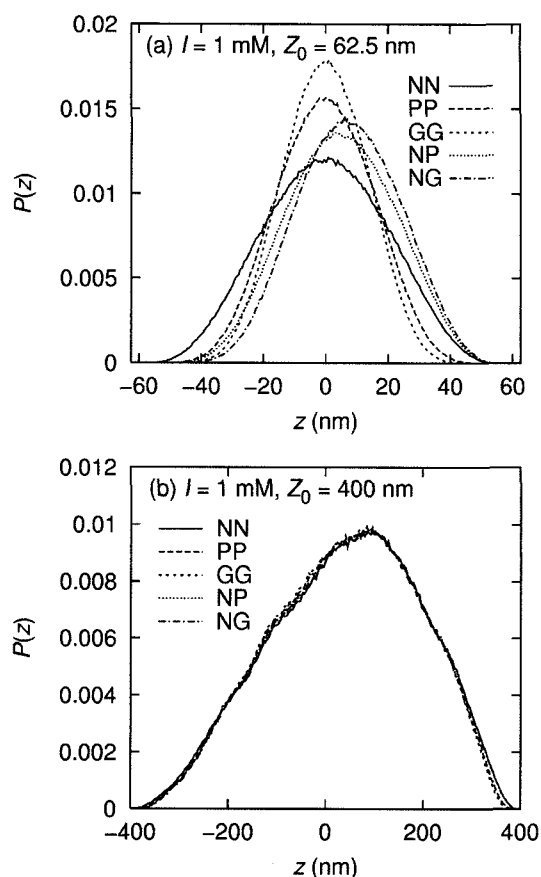

Fig. 6. The distribution of polyelectrolyte beads across the slit channel at (a) $I = 1$ mM and $Z_0 = 62.5$ nm and (b) $I = 1$ mM and $Z_0 = 400$ nm, where $\kappa^{-1} = 9.6$ nm at $I = 1$ mM. In asymmetric NP and NG slits, the wall with negative z coordinate is charged.

place the NN channel as the least effective in producing large persistence length and the GG channel as the most effective. Moreover, the minima in l_P^{15} are all located at the same Z_0 between 200 and 400 nm regardless of the wall charge characteristics, in contrast with the location of structural transition observed at $I = 0.01$ mM (Fig. 5a) which exhibits a large change as the wall charge varies. Therefore, the wall-bead electrostatic interaction near these minima cannot be uniform over the entire chain and is likely to be in effect only when a part of the chain, while performing the Brownian motion, happens to approach the wall within the Debye screening length. These explanations are consistent with our previous interpretation (Jeon and Chun, 2007) that both the nonmonotonic size variation and the loss of bond vector correlation are the result of local repulsive interactions between the wall and the terminal beads of the rotationally diffusing chain.

3.2. Polyelectrolyte distribution and diffusion in nano-channels

The distribution of a polyelectrolyte chain in the channel

provides direct information on the degree of confinement. Figs. 6 and 7 display the probability density $P(z)$ of the chain beads across the channel for the five slit channels considered. $P(z)$ was obtained by constructing the normalized histogram of z coordinates of all the beads in a polyelectrolyte chain over the trajectory in equilibrium. $P(z)$ of the NN channel at $I = 1$ mM and $Z_0 = 62.5$ nm (Fig. 6a) spans almost the entire channel width with depletion region of about 10 nm near the wall. This curve is very close to the distribution at $I = 100$ mM, where the five channels produce identical $P(z)$ (data not shown). In the symmetrically charged PP and GG channels, the distribution significantly narrows down and the depletion region extends twice to ~20 nm. In the asymmetric NP and NG channels, a noticeable shift of ~10 nm toward the neutral wall can be seen. Fig. 6b shows the distribution in a wider channel of $Z_0 = 400$ nm. Unlike in Fig. 6a, the distribution is now insensitive to different wall charges and all five curves are nearly identical. The bead distribution in this case is not symmetric which indicates the possibility of insufficient sampling. It would require a much longer sim-
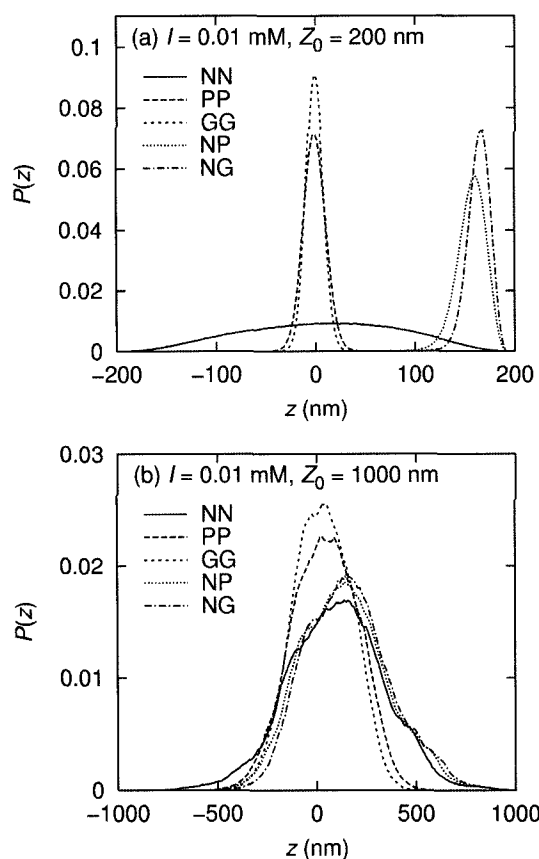
Fig. 7. The distribution of polyelectrolyte beads across the slit channel at (a) I = 0.01 mM and Z_0 = 200 nm and (b) I = 0.01 mM and Z_0 = 1000 nm, where κ^{-1} = 96 nm at I = 0.01 mM. In asymmetric NP and NG slits, the wall with negative z coordinate is charged.

ulation to resolve this issue in wide channels. Despite this uncertainty, it is evident that the wall charge density affects the polyelectrolyte distribution significantly even in channels with width an order of magnitude larger than the Debye screening length (κ^{-1} = 9.6 nm at I = 1 mM). The chain distributions at I = 0.01 mM in Fig. 7 demonstrate even more dramatic wall charge effect. In a slit four times wider than the Debye screening length (κ^{-1} = 96 nm at I = 0.01 mM) in Fig. 7a, the flat distribution in the NN channel is narrowed by ~80% in charged channels. Moreover, the chain migration away from the negatively charged wall in the case of NP and NG channels is considerable, with the chain occupying less than 25% of the total channel width. Once again, the extent of migration is much larger than the range of Debye screening. The narrow-down and shift of distribution still persists at the channel width Z_0 = 1000 nm in Fig. 7b.

Finally, Fig. 8 shows the two-dimensional self-diffusion coefficients D_T^{2D} of a polyelectrolyte chain in silts with different wall charges. As in the structural parameters in Section 3.1, the wall charge effect on D_T^{2D} is largest at I = 0.01
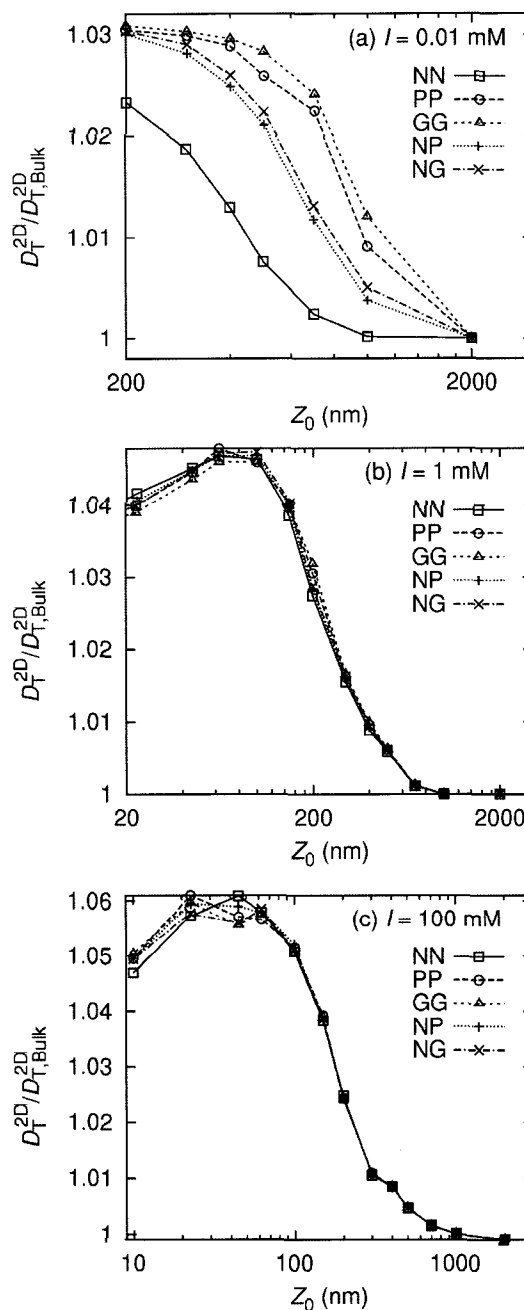

Fig. 8. Two-dimensional diffusion coefficient D_T^{2D} of a confined polyelectrolyte, scaled by the corresponding bulk value, as a function of the half slit width Z_0. D_T^{2D} only reflects displacement parallel to the walls.

mM (Fig. 8a) and is negligible at I = 100 mM (Fig. 8c). We note that D_T^{2D} increases with stronger confinement in Fig. 8a because the bead-wall hydrodynamic interaction is not included in the present BD simulation and the chain diffusion reflects only configurational effect of confinement. As explained in our previous study (Jeon and Chun, 2007), confined chains in the absence of bead-wall hydrodynamic interaction can diffuse faster parallel to the walls compared

to a chain in free space because its cross-sectional area normal to the direction of movement is on average smaller. This indicates that the hydrodynamic effect provides the main contribution to the hindered diffusion of confined chains. A full description of the hydrodynamic interaction including the wall effect is currently underway.

4. Conclusions

The structure of a polyelectrolyte chain confined in a slit nanochannel is affected by the wall charge density of the channel. In this paper, the neutral and two negatively charged surfaces of PDMS and glass were employed to investigate their effect on the confined polyelectrolyte behavior. It was found that the loss of long-range bond vector correlation is higher in more negatively charged channels and it could be inferred that this behavior arises from the local electrostatic interaction between the chain terminal beads and the wall. As expected, the wall charge effect is found to be greatest at low ionic strength. However, it is not negligible even at the modest ionic strength of 1 mM. The asymmetrically charged slit can induce migration of the polyelectrolyte toward a less repulsive wall as well as a narrow-down of chain distribution across the channel. These results suggest that the surface treatment of channels can be a useful method to confine and extend polyelectrolytes without sophisticated fabrication processes.

The computational methods employed in this study can be improved in the following directions: i) inclusion of explicit counterions to account for nonuniform distribution of medium charge and its fluctuations and, on a related note, a description of electrostatic interaction with full Poisson-Boltzmann level, ii) inclusion of hydrodynamic interaction between the chain and the wall to describe the behavior under flow and relevant rheological properties.

Acknowledgments

References

Allison, S.A., 1986, Brownian dynamics simulation of wormlike chains: Fluorescence depolarization and depolarized light scattering, *Macromolecules* **19**, 118-124.

Brochard-Wyart, F., T. Tanaka, N. Borghi and P.-G. de Gennes, 2005, Semiflexible polymers confined in soft tubes, *Langmuir* **21**, 4144-4148.

Chen, Y.L., M.D. Graham, J.J. de Pablo, G.C. Randall, M. Gupta

and P.S. Doyle, 2004, Conformation and dynamics of single DNA molecules in parallel-plate slit microchannels, *Phys. Rev. E* **70**, 060901-4.

Chun, M.-S. and O.O. Park, 1994, On the intrinsic viscosity of anionic and nonionic rodlike polysaccharide solutions, *Macromol. Chem. Phys.* **195**, 701-711.

Chun, M.-S. and S. Lee, 2005, Flow imaging of dilute colloidal suspension in PDMS-based microfluidic chip using fluorescence microscopy, *Colloids Surf. A* **267**, 86-94.

Cordeiro, C.E., M. Molisana and D. Thirumalai, 1997, Shape of confined polymer chains, *J. Phys. II France* **7**, 433-447.

Daoud, M. and P.-G. de Gennes, 1977, Statistics of macromolecular solutions trapped in small pores, *J. Phys. France* **38**, 85-93.

Doi, M. and S.F. Edwards, 1986, *The Theory of Polymer Dynamics*, Clarendon, Oxford.

Ermak, D.L. and J.A. McCammon, 1978, Brownian dynamics with hydrodynamic interactions, *J. Chem. Phys.* **69**, 1352-1360.

Fernandes, M.X., M.L. Huertas, M.A.R.B. Castanho and J. Garcia de la Torre, 2000, Conformation and dynamic properties of a saturated hydrocarbon chain confined in a model membrane: A brownian dynamics simulation, *Biochim. Biophys. Acta* **1463**, 131-141.

Hernandez-Ortiz, J.P., J.J. de Pablo and M.D. Graham, 2007, Fast computation of many-particle hydrodynamic and electrostatic interactions in a confined geometry, *Phys. Rev. Lett.* **98**, 140602/1-4.

Hur, J.S., E.S.G. Shaqfeh and R.G. Larson, 2000, Brownian dynamics simulations of single DNA molecules in shear flow, *J. Rheol.* **44**, 713-742.

Jendrejack, R.M., D.C. Schwartz, J.J. de Pablo and M.D. Graham, 2004, Shear-induced migration in flowing polymer solutions: Simulation of long-chain DNA in microchannels, *J. Chem. Phys.* **120**, 2513-2529.

Jeon, J. and M.-S. Chun, 2007, Structure of flexible and semi-flexible polyelectrolyte chains in confined spaces of slit micro/nanochannels, *J. Chem. Phys.* **126**, 154904/1-10.

Jian, H., A.V. Vologodskii and T. Schlick, 1997, A combined wormlike-chain and bead model for dynamic simulations of long linear DNA, *J. Comput. Phys.* **136**, 168-179.

Jo, K., D.M. Dhingra, T. Odijk, J.J. de Pablo, M.D. Graham, R. Runnheim, D. Forrest and D.C. Schwartz, 2007, A single-molecule barcoding system using nanoslits for DNA analysis, *Proc. Natl. Acad. Sci. U.S.A.* **104**, 2673-2678.

Manning, G.S., 1969, Limiting laws and counterion condensation in polyelectrolyte solutions: I. Colligative properties, *J. Chem. Phys.* **51**, 924-933.

Odijk, T., 1983, On the statistics and dynamics of confined or entangled stiff polymers, *Macromolecules* **16**, 1340-1344.

Öttinger, H.C., 1996, *Stochastic Processes in Polymeric Fluids: Tools and Examples for Developing Simulation Algorithms*, Springer, Heidelberg.

Paradossi, G. and D.A. Brant, 1982, Light scattering study of a series of xanthan fractions in aqueous solution, *Macromolecules* **15**, 874-879.

Rotne, J. and S. Prager, 1969, Variational treatment of hydro-

dynamic interaction in polymers, *J. Chem. Phys.* **50**, 4831-4837.

Russel, W.B., D.A. Saville and W.R. Schowalter, 1989, *Colloidal Dispersions*, Cambridge University Press, Cambridge.

Sato, T., T. Norisuye and H. Fujita, 1984, Double-stranded helix of xanthan: Dimensional and hydrodynamic properties in 0.1 M aqueous sodium chloride, *Macromolecules* **17**, 2696-2700.

Sho, T., T. Sato and T. Norisuye, 1986, Viscosity behavior and persistence length of sodium xanthan in aqueous sodium chloride, *Biophys. Chem.* **25**, 307-313.

Tran-Canh, D. and T. Tran-Cong, 2004, Element-free simulation of dilute polymeric flows using Brownian Configuration Fields, *Korea-Australia Rheology J.* **16**, 1-15.

van Vliet, J.H. and G. ten Brinke, 1990, Orientation and shape of flexible polymers in a slit, *J. Chem. Phys.* **93**, 1436-1441.

Wang, Y. and I. Teraoka, 2000, Structures and thermodynamics of nondilute polymer solutions confined between parallel plates, *Macromolecules* **33**, 3478-3484.

Warner, H.R., Jr., 1972, Kinetic theory and rheology of dilute suspensions of finitely extendible dumbbells, *Ind. Eng. Chem. Fund.* **11**, 379-387.